Research Square

Preprints are preliminary reports that have not undergone peer review.
They should not be considered conclusive, used to inform clinical practice,
or referenced by the media as validated information.

Impaired skeletal muscle development and regeneration in adenosine A2A receptor knockout mice

Zsuzsa Szondy

szondy@med.unideb.hu

University of Debrecen https://orcid.org/0000-0001-8347-9552

Albert Papp

University of Debrecen

Péter Szentesi

University of Debrecen

Dávid Deák

University of Debrecen

László Csernoch

University of Debrecen

Maysaa Ali

University of Debrecen

Zsolt Sarang

University of Debrecen

Article

Keywords:

Posted Date: November 12th, 2026

DOI: https://doi.org/10.21203/rs.3.rs-11353523/v1

License: This work is licensed under a Creative Commons Attribution 4.0 International License.
Read Full License

Additional Declarations: (Not answered)

Abstract

Skeletal muscle regeneration is orchestrated by an interplay of several cell types. It is initiated by local inflammation triggered by the dying cells, and involves phagocytosis of dead cells at the site of injury. Efferocytosis regulates the inflammatory program in macrophages by initiating the conversion of their inflammatory phenotype into the reparative one. While pro-inflammatory cytokines produced by them induce satellite cell proliferation and differentiation into myoblasts, growth factors (GDF3 and IGF-1) released by the reparative macrophages drive myoblast fusion and myotube growth. IGF-1 is also produced by differentiating myoblasts. Adenosine is generated from ATP released by dead cells following tissue injury. It mediates its physiological effects via four types of adenosine receptors. Among these, adenosine A2 receptors (A2Rs) expressed by myoblasts and macrophages increase adenylate cyclase activity, A2ARs being activated by moderately increased, while A2BRs by high concentrations of adenosine. Here we report that A2AR ablation results in decreased muscle weights, generation of small-sized myofibers in fast-twitch Nur77-expressing muscles, and alterations in muscle force generation in $A2AR^{-/-}$ mice. Following cardiotoxin-induced injury, fewer inflammatory cells transmigrated to the injury site, the dead cell clearance and the conversion of $Ly6C^{high}$ inflammatory macrophages to $Ly6C^{low}Nur77^{+}GDF3^{+}$ and to $Ly6C^{low}Nur77^{+}MHCII^{high}$ cells were delayed, the *Igf1* and *Gdf3* expressions decreased, myoblast fusion was impaired and the size of regenerating fibers was smaller in the tibialis anterior muscle of $A2AR^{-/-}$ mice. In contrast, stimulation of A2ARs facilitated myoblast fusion in differentiating C2C12 myoblasts by promoting their *Igf1* expression, while administration of an A2BR agonist to promote A2R signaling following cardiotoxin-induced injury stimulated myofiber fusion and growth in wild-type mice in a Nur77-dependent manner. Our data indicate that A2Rs play a key role in determining the myofiber size during development and the response to tissue injury, consequently A2BR agonists could be used to facilitate skeletal muscle regeneration.

Introduction

Skeletal muscle is one of the few organs that are capable of full regeneration following injury [1]. This is related to the fact that skeletal muscle contains muscle stem cells, the $Pax7^{+}$ satellite cells (SC), which are essential for the regeneration process. However, muscle regeneration is not a cell-autonomous process, since activation and differentiation of the SCs require continuous interaction with various cell types present or appearing at the site of tissue injury [2]. The regeneration process begins with the degeneration of injured myofibers, which release various danger-associated molecules recognized by cells within the skeletal muscle tissue, such as tissue-resident macrophages (MΦs) [3] and mast cells [4]. In response, mast cells degranulate [4], while tissue-resident MΦs actively secrete chemoattractants, such as macrophage-inflammatory proteins (MIPs), to recruit neutrophils [5] and further mast cells [6], generating an inflammatory milieu [7, 8]. These infiltrating cells initiate the removal of the injured myofibers at the site of tissue damage. In addition, they also secrete various types of pro-inflammatory cytokines to recruit more immune cells such as $Ly6C^{high}$ monocytes which, once they appear, start their differentiation into inflammatory $Ly6C^{high}$ MΦs [2]. Infiltrating inflammatory $Ly6C^{high}$ MΦs are the main

players in cell clearing, and release further pro-inflammatory cytokines, contributing also to the formation of the inflammatory environment required for proper SC proliferation [7, 8].

Tissue-resident MΦs and mast cells also contribute to initiation of the activation of SCs by triggering the asymmetric cell division of SCs which, after being differentiated into myoblasts, fuse together to form the new myofibers [9, 10]. While the pro-inflammatory cytokines TNF-α, interleukin-1β (IL-1β), and IL-6 promote SC proliferation [11], the differentiation or fusion of myoblasts are driven by growth factors like transforming growth factor (TGF)-β[12], insulin-like growth factor (IGF)-1[13] or growth differentiation factor 3 (GDF3) [14] released by reparative Ly6C^{low} MΦs that are formed from the Ly6C^{high} inflammatory MΦs during the efferocytosis process [15]. Several cytokines (such as TNF-α, IL-6, TGF-β, and IGF-1) are also produced by the myoblasts themselves, contributing to the regulation of their proliferation and differentiation in an autocrine manner [16].

The composition of the forming Ly6C^{low} MΦs is dynamically changing during the repair process, and based on single-cell mRNA expression analysis, they can be divided at least into three subpopulations each of which contributes specifically to the tissue repair: growth factor-expressing, resolution-related, and antigen-presenting MHCII^{high,} cells [17]. Since some of them express genes in a subpopulation-dependent manner, the loss of the proteins encoded by these genes individually affects the further conversion of the different Ly6C^{low} MΦ subpopulations [18–20].

Adenosine is a purine nucleoside, which is either released from cells or is formed extracellularly from the breakdown of adenosine nucleoside triphosphate (ATP). Following injury, a sharp increase in tissue adenosine concentrations was reported from basal nanomolar concentrations to micromolar concentrations [21]. Adenosine is then either taken up by the surrounding cells or is converted to inosine by the adenosine deaminase enzyme [22]. While being present, adenosine has been shown to mediate its effects via four types of adenosine receptors, which are all 7-transmembrane receptors but differ in their affinity for adenosine and in the G protein they interact with [23]. Adenosine A_1 receptors are stimulated by 10^{-10}-10^{-8} M concentrations of adenosine and mediate decreases in intracellular cyclic AMP (cAMP) levels, adenosine A_{2A} (A2ARs) and A_{2B} receptors (A2BRs) are stimulated by higher (5×10^{-7} M and 1×10^{-5} M, respectively) concentrations of adenosine and mediate increases in cAMP levels, while adenosine A_3 receptors (A3Rs) are stimulated by 10^{-6} M concentrations of adenosine and mediate adenylate cyclase inhibition. Since these receptors are expressed by nearly all inflammatory cells [21], the capillary endothelial cells [24], and the myoblasts themselves [25], adenosine might affect every aspect of the regeneration of skeletal muscle following injury.

In the present study it was investigated how the loss of A2ARs affects the skeletal muscle regeneration program in mice. As this receptor is activated by lower concentrations of adenosine, it is expected to be activated as soon as the injury occurs, and might be activated during later phases of the regeneration as well, since skeletal muscle cells are capable of generating adenosine [26, 27].

Materials and methods

Materials

All reagents were obtained from Merck, (Darmstadt, Germany) except when indicated otherwise.

Experimental animals

Experiments were carried out using 3–6-month-old young adult male FVB *Adora2a*$^{+/+}$ (A2AR$^{+/+}$) mice and their full-body *Adora2a*$^{-/-}$ (A2AR$^{-/-}$) littermates [28]. In some experiments *Nur77*$^{+/+}$ and *Nur77*$^{-/-}$ mice [29] were also used. Mice were bred in the heterozygous form under specific pathogen-free conditions in the central animal facility of the University of Debrecen. All animal experiments were approved by the Animal Care and Use Committee of the University of Debrecen, with permission number 7/2021/DEMÁB.

Cardiotoxin-induced muscle injury model

Mice were anesthetized with 2.5% isoflurane using a SomnoSuite device. To induce muscle damage, 50 µL of 12 µM cardiotoxin (CTX) (Latoxan, Valence, France), dissolved in phosphate-buffered saline (PBS) was injected into the tibialis anterior (TA) muscle. In some experiments, wild-type mice were injected BAY 60-6853, an A2B receptor agonist (2mg/kg), for the first 6 days during regeneration. The size of the treated groups was the same as reported by others in similar experiments [30]. There were no inclusion or exclusion criteria used in the selection of the A2AR$^{+/+}$ or A2AR$^{-/-}$ animals. Animals from each cage were randomly allocated to the CTX treatment, but no blinding was used. Muscles were harvested at various time points following injury, weighed, and processed for further experiments.

Bone marrow transplantation

Recipient A2AR$^{-/-}$ and A2AR$^{+/+}$ wild-type mice (7-week-old, males) were irradiated with 11 Gy using a Theratron 780C cobalt unit for the ablation of the recipient bone marrow. The animals to be irradiated were immobilized using a circular cage that could hold up to 11 mice. Following irradiation, isolated bone marrow cells (in sterile RPMI-1640 medium) flushed out from the femur, tibia, and humerus from donor A2AR$^{-/-}$ and A2AR$^{+/+}$ mice were transplanted into the recipient mice by retro-orbital injection (20 × 10^6 bone marrow (BM) cells per mouse). After 30 days of recovery, which in our hands results in higher than 95% repopulation [24, 31], TA muscle injury was induced by CTX injection. Mice were sacrificed by isoflurane overdose, muscle TA muscles were collected for histological analysis, while the CD45$^+$ cells were collected for FACS and gene expression analysis.

Hematoxylin/eosin and immunofluorescent staining of muscles

TA, extensor digitorum longus (EDL) and soleus (SOL) muscles from control mice or TA muscles at the indicated days post-injury were dissected for histological assessment. The muscles were snap-frozen in liquid nitrogen-cooled isopentane and kept at − 80°C. Seven-micrometer thick cryosections were cut at − 20°C using a 2800 Frigocut microtome (Leica, St Jouarre, France) and were kept at − 20°C until further

analysis. Hematoxylin/eosin (H&E) staining was performed to assess the overall morphology and presence of necrotic fibers following injury. Images from the sections were taken using an AMG EVOS cl microscope (Thermo-Fisher Scientific). To calculate the cross-sectional areas (CSA) and collagen-stained areas, frozen muscle sections were incubated in 10 mM citric acid-sodium citrate buffer (pH 6.0) for 15 min, then in blocking solution (50% FBS in PBS) for 1 h at room temperature. After blocking, samples were labeled with Dylight-488 conjugated anti-laminin B (PA5-22901, Invitrogen, Carlsbad, CA, USA) (1:100) and anti-collagen 1 antibody (SAB4500362) (1:100) at 4°C overnight followed by Alexa Fluor 488 conjugated Goat anti-Rabbit IgG secondary antibody followed by washing three times with PBS. The nuclei were labeled with 4 µg/mL Hoechst 33342 (NucBlue) (Invitrogen), and the slides were mounted with glass coverslips. Images were taken on a FLoid Cell Imaging Station fluorescent microscope (Thermo-Fisher Scientific) and analyzed using ImageJ v1.52 software (National Institutes of Health, Bethesda, MD, USA) with a muscle morphometry plugin. Areas containing fibers with centrally-located nuclei were considered regenerating muscle parts. CSAs are reported in μm^2, while collagen content is reported as the percentage of the total examined regenerating area.

Quantification of necrotic regions

Necrotic region was defined as an area containing myofibers infiltrated by basophilic single cells and quantified as described previously [17]. Briefly, 4 non-overlapping microscope view field areas were digitally captured from 6–8 H&E-stained TA muscle sections at 200-fold magnification. The percentage of necrotic area relative to the total regenerating area was calculated after manual outlining of the necrotic regions in the sections.

Isolation of muscle-derived $CD45^+$ cells

Muscle-derived cell isolation was carried out as described previously [32]. Briefly, control and regenerating TA muscles were removed and dissociated in RPMI containing 0.2% collagenase II (Thermo-Fisher Scientific) at 37°C for 1 hour and filtered stepwise through 100 µm and 40 µm filters. $CD45^+$ cells were labeled with microbeads and isolated using magnetic sorting columns (Miltenyi Biotec, Gladbach, Germany, catalog numbers: 130-052-301). The purity of isolated cells (around 95%) was determined by FACS analysis following staining them with phycoerythrin (PE)-conjugated antibodies against mouse CD45.2 (109807, BioLegend).

Quantification of intramuscular immune cells by flow cytometry

The magnetically separated muscle-derived $CD45^+$ cells were stained with Alexa Fluor 488-conjugated anti-F4/80 antibody (MF48020, Invitrogen) at room temperature for 15 min. The cells were gated based on their forward and side scatter characteristics. Macrophages were gated as $F4/80^+$ cells. $F4/80^+$ macrophages were also analyzed for expression of Ly6C, CD206, or major histocompatibility complex (MHC)II, following staining with the corresponding antibodies, Ly6C PerCP-Cy5.5 (128012, BioLegend),

CD206-PE (141705, BioLegend), or MHCII-FITC (107605, BioLegend), respectively. Fluorescent intensity was measured on a Becton Dickinson FACSCalibur instrument (Becton, Dickinson and Company).

Gene expression analysis

Total RNA of muscle-derived $CD45^+$ cells and TA muscles homogenized in TRIzol with a Shakeman homogenizer (BioMedical Science, USA) was isolated with TRIzol reagent (Invitrogen), according to the manufacturer's instructions. Total RNA was reverse transcribed into cDNA using a High Capacity cDNA Reverse Transcription Kit (Thermo-Fisher Scientific), according to the manufacturer's instructions. Quantitative RT-PCR was carried out in triplicate using FAM-labeled MGB assays (Thermo-Fisher Scientific) on a Roche LightCycler LC 480 real-time PCR instrument (Roche, Basel, Switzerland). Relative mRNA levels in the case of $CD45^+$ cells were calculated using the comparative C_T method and normalized to beta-actin (β-actin) mRNA. In the case of the TA muscle samples, gene expression was normalized to the total RNA content (200 ng) of the samples. Catalog numbers of the TaqMan assays used were the following: *Adora3* Mm07296455_m1, *Adora2a* Mm00802075_m1, *Adora2b* Mm00839292_m1, *Ccl2/Mcp1* Mm00441242_m1, *Tnfa* Mm00443258_m1, *Il1b* Mm00434228_m1, *Il6* Mm00446190_m1, *Igf1* Mm00439560_m1, *Tgfb1* Mm01178820_m1, *Gdf3* Mm00433563_m1, *Pax7* Mm00834082_m1, *Myod1* Mm00440387_m1, *Myog* Mm00446194_m1, *Nr4a1/Nur77* Mm01300401_m, and *Actb* Mm02619580_g1.

C2C12 cell culture and differentiation

Murine myoblast C2C12 cells were obtained from American Type Culture Collection (ATCC; CRL-1772), and were maintained according to the company's instructions. In brief, cells were cultured in Dulbecco's modified Eagle's medium (DMEM) supplemented with 20% fetal bovine serum (FBS), 100 U/mL penicillin, and 100 µg/mL streptomycin (growth medium) at 37°C in 5% CO2 and 95% air at 100% humidity. The absence of mycoplasma was tested using the PCR Mycoplasma Test Kit I/C (PromoCell, Heidelberg, Germany). Cells were plated into 48-well plates at a density of 3500 cells/cm2. For the 6-day differentiation period, the cells were plated on a collagen-coated surface and cultured in DMEM medium containing 2% FBS and 1% ITS (insulin, transferrin, sodium selenite), replaced every 2nd day with a fresh one. During differentiation, cells were treated daily with 1 µM of the selective A2AR agonist CGS 21680 hydrochloride (TargetMol Chemicals, Boston, MA, USA), dissolved in DMSO, while control cells received daily 0.05% (v/v) DMSO. Cells were collected in TRIzol on each day of differentiation, and *Igf1* expression levels were determined as described in the gene expression analysis section. In addition, the fusion index of myoblasts was assessed on day 6 of differentiation. To test the involvement of the orphan nuclear receptor Nur77 in A2AR signaling, CGS21680 was also added in the presence of 5 µM DIM-C-pPhOH (C-DIM8) (TargetMol), a Nur77 antagonist.

Immunostaining of C2C12 cells

For MYH4 staining, 6-day differentiated C2C12 cells in 48-well plates were fixed with ice-cold methanol for 15 min at 4°C, washed three times with PBS, and then blocked with PBS/5% FBS/0.3% Triton X-100

for 60 min at room temperature. Alexa Fluor 488-conjugated anti-Myosin heavy chain 4 (Thermo Fisher Scientific) was added at a 1:100 dilution in PBS/1% bovine serum albumin/0.3% Triton X-100 for 12 h at 4°C. After staining, cells were rinsed three times in PBS and counterstained with NucBlue according to the manufacturer's instructions for DNA staining. Fluorescent and bright-field pictures were taken on a FLoid Cell Imaging Station fluorescent microscope. To evaluate myoblast fusion, digitally captured photos were analyzed using ImageJ software. The fusion index was calculated by expressing the number of nuclei within MYHC4-positive myotubes with ≥ 3 nuclei as a percentage of the total nuclei.

In Vivo Assessment of Muscle Force

Forelimb grip force was measured as previously described [33]. Briefly, mice were trained until they consistently grasped the horizontal bar of a grip-strength meter. Each animal was then gently pulled horizontally away from the bar, and the peak force exerted immediately prior to release was recorded. Force signals were digitized at 2 kHz. Ten to fifteen trials were performed per animal and the recordings for each mouse were used to generate a single representative data point. Grip testing was performed on the day of sacrifice for all groups.

Voluntary wheel running

Mice were singly housed with a running wheel (Campden Instruments Ltd., Loughborough, UK). Wheel revolutions were recorded continuously to a computer in 20-minute bins for 14 consecutive days. For each mouse, daily metrics (total distance, mean speed, maximum speed, and total running duration) were calculated and subsequently averaged within experimental groups.

Ex vivo muscle contractile measurements

Isolated muscle contractile properties were assessed as described [33]. Dissected muscles were mounted horizontally in an experimental chamber superfused continuously at 10 mL/min with Krebs solution (mM: NaCl 135, KCl 5, CaCl2 2.5, MgSO4 1, HEPES 10, NaHCO3 10, glucose 10; pH 7.2) at room temperature and equilibrated with 95% O2/5% CO2. One tendon was attached to a fixed support and the opposite tendon to a capacitive mechano-electric force transducer. Two platinum electrodes were positioned beneath the muscle to deliver supramaximal pulses (2 ms duration) for single-twitch stimulation. Force responses were digitized at 2 kHz using a Digidata 1200 A/D interface and analyzed with AxoTape software (Axon Instruments, Foster City, CA,

USA). Muscle length was adjusted to the length producing maximal twitch force, and preparations were equilibrated for 5 minutes. Single twitches were evoked at 0.5 Hz, and at least ten consecutive twitches were recorded; mean twitch amplitude was used for analysis when amplitude variability within the train was < 3%. Tetanic contractions were elicited using 200 Hz stimulation for 200 ms for EDL and 100 Hz for 500 ms for soleus SOL. Time-to-peak (TTP) and half relaxation time (time from peak to 50% of maximal force) were calculated for individual twitches and tetani. Fatigue protocols and force–frequency relationships were performed as described earlier [33].

Statistical analysis

All the data are representative of at least three independent experiments, and all data are expressed as individual values and mean or mean ± SD, except those for the physiological parameters of muscles, which are expressed as mean ± SEM. Normal distribution of the data was tested using the online tool https://www.statscalculators.com/calculators/chart/qq-plot. Statistical analysis was performed using two-tailed, unpaired Student's t-test for two-group tests with normal data distribution and Mann–Whitney U-test for non-normal distribution samples, and one-way ANOVA with post-hoc Tukey HSD test for multiple comparisons. The equal variance of the samples was tested by F-test. Statistical analysis was carried out using GraphPad Prism. *$p < 0.05$, **$p < 0.01$, ***$p < 0.001$, and ****$p < 0.0001$.

Results

Impaired tissue regeneration in the TA muscles of $A2AR^{-/-}$ mice following CTX-induced muscle injury

To study the role of A2AR in skeletal muscle regeneration, we performed histological analysis of control and CTX-injected TA muscles of wild-type and $A2AR^{-/-}$ mice [28]. There was no obvious difference in the gross appearance between the control muscles (Fig. 1). On days 2, 3 and 4 both $A2AR^{+/+}$ and $A2AR^{-/-}$ regenerating muscles displayed local necrosis and abundant inflammatory cell infiltration. However, by day 10, when most of the necrotic fibers were cleared from the control muscles, large necrotic areas were still detectable in the $A2AR^{-/-}$ muscles. This finding was unexpected, because clearance efficiency is generally associated with the efferocytosis capacity of macrophages [31], but the loss of A2ARs does not affect the phagocytosis of dead cells [34]. By day 22 post-injury, the overall histological architecture of both $A2AR^{+/+}$ and $A2AR^{-/-}$ muscles had been largely restored, and necrotic fibers were no longer visible (Fig. 1, Fig. 2A).

Efficient muscle repair requires the temporary deposition of extracellular matrix proteins which stabilize the healing tissue and provide a protein scaffold for the growing myofibers, however, later they are degraded. Accordingly, we detected an increased amount of collagen I at day 10 in the regenerating muscles of both $A2AR^{+/+}$ and $A2AR^{-/-}$ mice as compared to their own non-regenerating muscles. In addition, we found prolonged collagen I deposition in the $A2AR^{-/-}$ muscles as compared to the $A2AR^{+/+}$ ones in line with the delayed clearance of the necrotic areas (Fig. 2B and C).

To further characterize the muscle regeneration in the absence of A2ARs, we compared the muscle weights and the myofiber CSAs of vehicle- and CTX-treated TA muscles from $A2AR^{+/+}$ and $A2AR^{-/-}$ mice. TA muscle weights were not different between control and regenerating muscles at day 10 or 22 post-injury in $A2AR^{-/-}$ mice as compared to the wild-type controls (Fig. 3A). The mean and median CSA of newly formed myofibers with central nuclei in $A2AR^{-/-}$ mice, however, were significantly smaller at both day 10 (Fig. 3B and C) and at day 22 post-injury (Fig. 3B and D). The CSA frequency distribution showed similar fiber size distribution in the$A2AR^{+/+}$ and $A2AR^{-/-}$ mice, but the frequency of smaller fibers was

significantly smaller, while that of bigger fibers was significantly higher in day 22 regenerating A2AR$^{-/-}$ muscles as compared to the wild-type ones (Fig. 3D).

The number of myofibers with two or more central nuclei is an indicator of myoblast fusion in the regenerating muscles. In accordance with the above data, the number of newly formed fibers with 2 or more central nuclei was significantly less in A2AR$^{-/-}$ mice as compared to wild-type mice both at day 10 and 22 post-injury (Fig. 3E). What is more, we did not detect an increase in the CSA or in myoblast fusion between day 10 and 22 in the A2AR$^{-/-}$ muscles. These data altogether indicated impaired skeletal muscle regeneration in the absence of A2ARs, characterized by delayed clearance of necrotic myofibers, by prolonged deposition of collagen I, by severely impaired myoblast fusion, and consequently by thinner myofibers produced.

Altered transmigration and delayed polarization of MΦs at the site of injury in the TA muscles of A2AR$^{-/-}$ mice

Next, we determined the characteristics of the transmigrated CD45^{+} cells in the TA muscles in A2AR$^{-/-}$ mice. As seen in Fig. 4A, less CD45^{+} cells transmigrated in the absence of A2ARs to the site of injury. Bone marrow transplantation experiments revealed that the degree of transmigration was altered by the loss of A2ARs of both the tissue resident and the bone marrow-derived cells (Fig. 4B).

While the loss of A2ARs did not affect the percentage of MΦs within the CD45^{+} population, that of neutrophils significantly increased (Fig. 4A). Loss of A2ARs in both the bone marrow-derived and tissue resident cells promoted neutrophil transmigration (Fig. 4B) in accordance with previous publications, which demonstrated that the cAMP signaling inhibits leukocyte transmigration [35]. In line with previous publications, which suggested that elevated intracellular cAMP levels promote the M1/M2 phenotypic change of MΦs [35], loss of A2ARs resulted in a delay in the phenotypic shift affecting dominantly the formation of the Ly6C^{low}MHCII^{high} antigen presenting population (Fig. 4C). Bone marrow transplantation experiments confirmed that this delay was indeed related to the loss of A2ARs in the bone marrow-derived cells (Fig. 4D).

Loss of A2ARs leads to enhanced *Il1b* and decreased *Gdf3* expression by transmigrating CD45^{+} cells

To characterize the behavior of transmigrating CD45^{+} cells in the absence of A2ARs, first we determined the mRNA expression of adenosine receptors in the wild-type and A2AR null cells at various time points following CTX-induced skeletal muscle injury. Previous work from our laboratory has shown that while both *Adora 2a* and *Adora 2b* genes are highly expressed by the pro-inflammatory population of MΦs, and later their expression is present but lower in the Ly6C^{low} population, *Adora 3* is dominantly expressed by the *Nur77*-positive resolution-related group of Ly6C^{low} MΦs [20, 24] (Fig. S1). As seen in Fig. 5A, *Adora 2b* showed the highest expression among the adenosine receptors. In line with its expression pattern in the MΦ populations, as the Ly6C^{high} Mφs converted with time to LyC6^{low} MΦs, the mRNA expression of both A2Rs decreased. In contrast, the expression of *Adora 3* increased with time, mirroring the formation of

the pro-resolving MΦ population. In the absence of A2ARs, we detected a compensatory increase in the mRNA expression of A2BRs in the pro-inflammatory day 2 $CD45^+$ cell population, while less *Adora 3* was expressed at day 4, together with a significant drop in *Nur77* expression on the same day (Fig. 5C). These data indicate that A2ARs contribute to the proper generation of those pro-resolving MΦs, which are characterized by both *Adora 3* and *Nur77* expressions (Fig. S1) [20, 24].

Next, we determined the mRNA expressions of various pro-inflammatory cytokines and growth factors produced by the $CD45^+$ cells. As seen in Fig. 5B, we did not find a change in the mRNA expressions of *Ccl2/Mcp1, Tnfa*, or *Il6*, however, that of *Il1b* was significantly increased at day 2, when pro-inflammatory MΦs are present in high amounts. In contrast, we did not find alterations in the mRNA expression of the anti-inflammatory *Il10*, in accordance with the observation that the percentage of the *Il10*-expressing $CD206^+$ MΦs [20] was not altered (Fig. 4C). The production of *Igf1* by $A2AR^{-/-}$ $CD45^+$ cells was not altered, but that of *Gdf3* was decreased. The production of GDF3 was reported to be induced by the Nur77 transcription factor [20], and the expression of *Nur77* was significantly decreased in the absence of A2ARs (Fig. 5C).

Loss of A2ARs leads to enhanced *Il1b* and *Il6* expression driving the proliferation of more SCs, but to decreased transcription of *Igf1* and *Gdf3*

Next, we determined the mRNA expression of adenosine receptors in the total skeletal muscle. As seen in Fig. 6A, we could confirm the compensatory increase in the mRNA expression of A2BRs at day 2 post-injury on skeletal muscle level as well. Loss of A2ARs did not alter the *Ccl2/Mcp1* expression confirming that A2ARs affect directly the transmigration of bone marrow-derived cells. The *Il1b* and *Il6* mRNA expressions, however, were elevated in $A2AR^{-/-}$ TA muscles (Fig. 6B). In contrast, the *Igf1* and *Gdf3* levels were decreased. Since neither *Il6* nor *Igf1* expressions were altered in the $CD45^+$ cells (Fig. 5B and C), these data indicate that A2ARs acting on the myoblasts might regulate the production of these myokines [36, 37].

The increased *Il6* and *Il1b* expression promoted the proliferation of SCs, as detected by the increase of the mRNA expressions of *Pax7*, and the differentiation markers *Myod1*, *Myog*, and *Myh7*, without affecting the rate of myoblast differentiation. Despite the increased number of myoblasts produced, the decrease in *Igf1* and *Gdf3* expression might explain the decrease in the myoblast fusion observed at day 10 post-injury (Fig. 3E).

A2Rs promote myoblast fusion by enhancing Nur77-mediated IGF-1 production

Since during the repair of skeletal muscle in the $A2AR^{-/-}$ mice, we did not see evidence for further fusion after 10 days post-injury (Fig. 3E), we also tested by using C2C12 myoblasts, whether activation of A2ARs by an agonist could affect myoblast fusion. We found that it does (Fig. 7A), very likely by promoting at least the expression of *Igf1* via the increasingly expressed A2ARs (Fig. 7B and C).

Since A2ARs located on both myoblasts and bone marrow-derived cells contribute to the proper regeneration, we tested whether addition of an A2BR agonist injected during the first 6 days following CTX-induced injury could affect skeletal muscle regeneration in wild-type mice. We selected the first 6 days because transmigrated cells can be detected during this period of time in the injured muscle together with myoblasts, and selected an A2BR agonist to inject, because A2ARs are very likely saturated by adenosine during the inflammatory phase, and as a result, no further response can be expected. As seen in Fig. 7D, peritoneal injection of an A2BR agonist significantly increased both the CSA of the generated myofibers and the myoblast fusion following injury.

Previous studies have shown that the Nur77 transcription factor is a main determinant of the myofiber size and muscle mass [38], it mediates its effects via inducing the expression of *Igf1* [38], and the adenylate cyclase pathway is a strong regulator its transcriptional activity in the skeletal muscle [39]. Though as compared to the $A2AR^{+/+}$ mice, we did not detect alterations in the Nur77 expression in the $A2AR^{-/-}$ muscles during regeneration following CTX-induced injury or in the A2AR agonist-treated C2C12 cells (data not shown), protein kinase A can directly enhance Nur77 transcriptional activity by promoting its coactivator binding [40]. That is why we tested by using $Nur77^{-/-}$ mice, whether A2R signaling involves Nur77. As shown in Fig. 7D, in the absence of Nur77, the A2BR agonist was unable to enhance the fiber size and myoblast fusion in $Nur77^{-/-}$ muscles. In addition, a Nur77 antagonist prevented the A2AR agonist-induced-increase in *Igf1* expression in C2C12 cells (Fig. 7E).

Loss of A2ARs affects the development of skeletal muscle

Since an A2AR agonist promoted the fusion of C2C12 myoblasts in the absence of MΦs, we decided to check whether loss of A2ARs affects the development of skeletal muscle in mice. There was a slight decrease in body weight, and in TA muscle weight in $A2AR^{-/-}$ mice as compared to the wild-type mice, while the EDL and SOL muscle weights did not change (Fig. 8A and B). The true significant difference was, however, found when the fiber CSAs were compared: a significantly smaller mean and median fiber CSAs in the TA and EDL (the two fast-twitch) muscles of $A2AR^{-/-}$ mice were detected as compared to wild-type ones. In contrast, no alteration was detected in the SOL (low-twitch) muscle (Fig. 8C-F).

Next, we determined whether the loss of A2ARs has an impact on the physical performance of $A2AR^{-/-}$ mice of 18–20 months of age. *In vivo* forelimb grip strength did not differ between genotypes, and grip force normalized to body weight showed no significant genotype-dependent difference either (Table S1). Voluntary wheel-running metrics (daily distance, mean speed, and maximum speed) were likewise unchanged, although $A2AR^{-/-}$ mice exhibited a significantly greater total running duration relative to wild-type controls (Table S2).

Ex vivo measurements revealed genotype-dependent deficits in maximal force generation of isolated EDL and SOL muscles (Table S3 and S4). In EDL, both twitch and tetanic forces were significantly reduced in $A2AR^{-/-}$ mice compared with $A2AR^{+/+}$ controls. In SOL, tetanic force was significantly decreased, whereas twitch force showed a smaller, nonsignificant reduction. Kinetic analyses indicated

faster tetanic rise times in both muscle types from A2AR$^{-/-}$ mice; SOL tetanic relaxation was accelerated, while EDL relaxation was prolonged. Twitches in A2AR$^{-/-}$ EDL also displayed a faster time-to-peak. Muscle fatigability did not differ between genotypes.

Force–frequency analysis demonstrated altered frequency-dependent force production in A2AR$^{-/-}$ muscles (Fig. 8G). Both EDL and SOL from A2AR$^{-/-}$ mice exhibited reduced tolerance to high-frequency stimulation. At low stimulation frequencies, significant genotype differences were apparent for both muscles, indicating a slower activation response in A2AR$^{-/-}$ preparations.

Discussion

At the site of injury, adenosine is generated from ATP released by the dying cells via the action of ectonucleotidases which are expressed on the surface of various cells in the skeletal muscle, such as MΦs [41], satellite cells [42], and myoblasts [43]. Thus, adenosine generated on the surface can directly engage the adenosine receptors, which are also expressed by these cells [44]. The amount of ATP released is strongly related to the degree of injury, and since the four types of adenosine receptors are activated in an adenosine concentration-dependent manner, adenosine receptors are capable of sensing the degree of damage and orchestrating the repair accordingly. In the present paper it was investigated how the skeletal muscle tissue repair is altered, if the A2ARs, which are activated by moderately elevated adenosine concentrations, are knocked out.

Our data demonstrate, that in response to tissue injury, fewer bone marrow-derived cells transmigrate to the injury site in the absence of A2ARs. It is very likely that fewer transmigrated cells cannot be fast enough in clearing cell debris, explaining the prolonged presence of necrotic areas in the injured A2AR$^{-/-}$ muscles. As long as the injured area is not cleared, collagen deposition cannot be properly built to provide a scaffold area for the growing new myofibers, also explaining the prolonged presence of collagen deposition in the injured A2AR$^{-/-}$ muscle tissues.

Though the number of transmigrating cells decreased, we detected an increased inflammatory response, especially a significantly elevated *Il1b* expression, at the site of skeletal muscle injury in A2AR$^{-/-}$ mice. We found that the enhanced inflammatory response was related to the fact that A2ARs, which are expressed primarily in a group of inflammatory Ly6C^{high} cells [24], following the phenotypic shift should trigger the proper Nur77 expression in the pro-resolving population of reparative macrophages. Nur77 has been known for a long time to mediate anti-inflammatory signaling [45], and we reported previously that *IL1b* and *Nur77* are co-expressed in the pro-resolving subpopulation of MΦs [20]. In addition, as we have shown by studying *Nur77*$^{-/-}$ mice [20], Nur77 also contributes to the efficient generation of the Ly6C^{low}MHCII^{high} antigen-presenting cells, explaining the observed delay in their formation in the A2AR$^{-/-}$ mice.

An enhanced inflammatory milieu promotes SC proliferation [11]. However, despite the increased number of new myoblasts, we detected the formation of thinner myofibers as a result of decreased fusion ability of A2AR$^{-/-}$ myoblasts. The decreased fusion ability of A2AR$^{-/-}$ myoblasts was partially related to the lower production of GDF3 by A2AR$^{-/-}$ CD45^{+} cells but also to the lower Nur77-dependent production of IGF-1 by the A2AR$^{-/-}$ myoblasts themselves. In support of this latter mechanism, we found that activation of the A2ARs by an A2AR agonist promoted the fusion of C2C12 myoblasts and also their *Igf1* expression. In this context, it is worth noting that the expression of pannexin1 channel which releases ATP [47], and the ATP-hydrolyzing activity of C2C12 myoblasts are known to be significantly increased around the time, when they fuse [48]. Thus, they are able to generate adenosine and trigger their own A2ARs via an autocrine mechanism to promote fusion.

If A2ARs are contributing to myoblast fusion, loss of A2ARs must affect the development of the skeletal muscle as well. That is why we investigated the phenotype of the A2AR-deficient skeletal muscles, and found that they indeed have decreased-size myofibers. Interestingly, however, this alteration in the phenotype was characteristic only of the fast-twitch muscles, whose metabolism and growth are strongly influenced by IGF-1 [45], and in which Nur77, a transcription factor that regulates myofiber size, is exclusively expressed [38].

Next, we tried to characterize functionally the A2AR$^{-/-}$ muscles. Deletion of A2AR produced a dissociation between whole-animal performance and intrinsic muscle contractility: grip strength and most voluntary running metrics were preserved, yet isolated EDL and SOL muscles showed reduced maximal force and altered contractile kinetics. The preserved *in vivo* strength likely reflects behavioral or systemic compensation (e.g., increased running duration observed in A2AR$^{-/-}$ mice), redundancy among neuromuscular or metabolic pathways, or the influence of intact neural, circulatory, and endocrine inputs that are absent in *ex vivo* preparations.

The reduction in tetanic force in both EDL and SOL, with a concurrent decrease in EDL twitch force, indicates that A2AR loss impairs the muscles' capacity to generate peak force. The differential effects on twitch versus tetanus and the muscle-specific changes in time-to-peak and relaxation suggest altered excitation–contraction coupling and/or calcium handling. Changes in sarcoplasmic reticulum Ca^{2+} release, reuptake kinetics, or sensitivity of the contractile apparatus to Ca^{2+} are plausible mechanisms that would produce the observed frequency-dependent deficits and the rightward shift in the force–frequency relationship at low stimulation frequencies.

The unaltered fatigability indicates that fatigue-resistant metabolic pathways remain largely intact, arguing against a primary deficit in mitochondrial ATP supply under the stimulation protocols used. Instead, the phenotype is more consistent with alterations in rapid contractile control (ion channel function, Ca^{2+}-ATPase activity, or regulatory protein phosphorylation) or subtle fiber-type shifts that reduce peak force but preserve endurance properties.

Finally, we tested how overstimulation of the A2R signaling affects myofiber growth in wild-type animals following CTX-induced skeletal muscle injury. We have already reported that A2BR stimulation enhances the number of transmigrating cells [24]. Now we report that exposing mice to an A2B receptor agonist during the first 6 days of tissue repair significantly increases both myoblast fusion and the myofiber size generated following CTX-induced injury in TA muscles in a Nur77-dependent manner. Altogether these data with our previously published ones [24] indicate that adenosine plays a major role in determining the myofiber size during development and regeneration, and we propose that stimulation of A2R signaling by A2B receptor agonists could be used in the treatment of skeletal muscle injuries.

Declarations

Conflict of interest

The authors state no conflict of interest.

Funding

This study was supported by the National Research, Development, and Innovation Office-NKFI, Hungary (138162).

Author contribution

A.B.P. performed most of the experiments and analyzed the data, P.Sz. and L.Cs. performed the muscle strength experiments, D.D. performed the bone marrow transplantations, M.A.A. contributed to the C2C12 cell experiments. Zs.S. supervised the experiments and prepared the figures, while Zs.Sz. designed the experiments, analyzed the data, wrote the paper and was responsible for funding acquisition.

Acknowledgements

We acknowledge Dr. Cathrine Ledent for providing the *Adora2*$^{-/-}$ mice and Dr. Jeffrey Milbrandt for providing the *Nur77*$^{-/-}$ mice. A.B.P was supported by the Count István Tisza Foundation for the University of Debrecen (GTIDEA) through the GTIDEA Excellence PhD Scholarship Programme. Maintenance of the mouse colonies and the animal work were performed in the Laboratory Animal Facility, Life Science Building, University of Debrecen. The technical assistance of Anikó Nagy is gratefully acknowledged.

Data availability

All the data generated or analyzed during this study are available from the corresponding author upon reasonable request.

References

1. Szondy Z, Al-Zaeed N, Tarban N, Fige E, Garabuczi E & Sarang Z. Involvement of phosphatidylserine receptors in skeletal muscle regeneration. Therapeutic implications. *J Cachexia Sarcopenia Muscle* 13, 1961–1973 (2022)
2. Deconinck N & Dan B. Pathophysiology of Duchenne muscular dystrophy: current hypotheses. *Ped Neurol* 36, 1–7 (2007)
3. Tu H & Li-Y L. Inflammation balance in skeletal muscle damage and repair. *Front Immunol* 14, 1133355 (2023)
4. Yang W & Hu P. Skeletal muscle regeneration is modulated by inflammation. *J Orthop Translat* 13, 25–32 (2018)
5. De Filippo K, Henderson RB, Laschinger M & Hogg N. Neutrophil chemokines KC and macrophage-inflammatory protein-2 are newly synthesized by tissue macrophages using distinct TLR signaling pathways. *J Immunol* 80, 4308–4315 (2008)
6. Draber P, Halova I, Polakovicova I & Kawakami T. Signal transduction and chemotaxis in mast cells. *Eur J Pharmacol* 778, 11–23 (2016)
7. Rigamonti E, Touvier T, Clementi E, Manfredi AA, Brunelli S & Rovere-Querini P. Requirement of inducible nitric oxide synthase for skeletal muscle regeneration after acute damage. *J Immunol* 190, 1767–1777 (2013)
8. Vezzoli M, Castellani P, Corna G, Castiglioni A, Bosurgi L, Monno A *et al.* High-mobility group box 1 release and redox regulation accompany regeneration and remodeling of skeletal muscle. *Antioxid Redox Signal* 15, 2161–2174 (2011)
9. Ratnayake D, Nguyen PD, Rossello FJ, Wimmer VC, Tan JL, Galvis LA *et al.* Macrophages provide a transient muscle stem cell niche via NAMPT secretion. *Nature* 591, 281–287 (2021)
10. Bentzinger CF, Wang YX, Dumont NA & Rudnicki MA. Cellular dynamics in the muscle satellite cell niche. *EMBO Rep* 14, 1062–1072 (2013)
11. Otis JS, Niccoli S, Hawdon N, Sarvas JL, Frye MA, Chicco AJ *et al.* Pro-inflammatory mediation of myoblast proliferation. *PLoS One* 9, e92363 (2014)
12. Zentella A & Massagué J. Transforming growth factor β induces myoblast differentiation in the presence of mitogens. *Proc Natl Acad Sci USA* 89, 5176–5180 (1992)
13. Tidball JG & Welc SS. Macrophage-Derived IGF-1 Is a Potent Coordinator of Myogenesis and Inflammation in Regenerating Muscle. *Mol Ther* 23, 1134–1135 (2015)
14. Varga T, Mounier R, Patsalos A, Gogolák P, Peloquin M, Horvath A *et al.* Macrophage PPARγ, a lipid activated transcription factor controls the growth factor GDF3 and skeletal muscle regeneration. *Immunity* 45, 1038–1051 (2016)

15. Chazaud B. Inflammation and skeletal muscle regeneration: leave it to the macrophages. *Trends Immunol* 6, 481–492 (2020)
16. Henningsen J, Rigbolt KTG, Blagoev B, Pedersen BK & Kratchmarova I. Dynamics of the skeletal muscle secretome during myoblast differentiation. *Mol Cell Proteomics* 9, 2482–2496 (2010)
17. Patsalos A, Halasz L, Medina-Serpas MA, Berger WK, Daniel B, Tzerpos P *et al.* A growth factor-expressing macrophage subpopulation orchestrates regenerative inflammation via GDF-15. *J Exp Med* 219, e20210420 (2022)
18. Al-Zaeed N, Budai Z, Szondy Z & Sarang Z. TAM kinase signaling is indispensable for the proper skeletal muscle regeneration process. *Cell Death Dis* 12, 611 (2021)
19. Budai Z, Al-Zaeed N, Szentesi P, Halász H, Csernoch L, Szondy Z et al. Impaired Skeletal Muscle Development and Regeneration in Transglutaminase 2 Knockout Mice. *Cells* 10, 3089 (2021)
20. Garabuczi E, Fige E, Tarban N, Patsalos A, Halász L, Szendi-Szatmári T *et al.* Nur77 and PPARγregulate transcription and polarization in distinct subsets of M2-like reparative macrophages during regenerative inflammation. *Front. Immunol.* 14, 1139204 (2023)
21. Haskó G & Cronstein B. Regulation of inflammation by adenosine. *Front Immunol* 4, 85 (2013)
22. Cristalli G, Costanzi S, Lambertucci C, Lupidi G, Vittori S, Volpini R *et al.* Adenosine deaminase: functional implications and different classes of inhibitors. *Med Res Rev* 21, 105–128 (2001)
23. Fredholm BB. International union of pharmacology. XXV. Nomenclature and classification of adenosine receptors, *Pharmacol Rev* 53, 527–552 (2001)
24. Tarban N, Papp AB, Deák D, Szentesi P, Halász H, Patsalos A *et al.* Loss of adenosine A3 receptors accelerates skeletal muscle regeneration in mice following cardiotoxin-induced injury. *Cell Death Dis* 14, 706 (2023)
25. Gnad T, Navarro G, Lahesmaa M, Reverte-Salisa L, Copperi F, Cordomi A *et al*. Adenosine/A2B Receptor Signaling Ameliorates the Effects of Aging and Counteracts Obesity. *Cell Metab* 32, 56–70.e7 (2020)
26. Bockman EL, Berne RM & Rubio R. Release of adenosine and lack of release of ATP from contracting skeletal muscle. *Pflugers Arch* 355, 229–241 (1975)
27. Langlois S & Cowan KN. Regulation of Skeletal Muscle Myoblast Differentiation and Proliferation by Pannexins. *Adv Exp Med Biol* 925, 57–73 (2017)
28. Ledent C, Vaugeois JM, Schiffmann N, Pedrazzini T, El Yacoubi M, Vanderhaeghen JJ et *al.* Aggressiveness, hypoalgesia and high blood pressure in mice lacking the adenosine A2a receptor. *Nature* 388, 674–678 (1997)
29. Lee SL, Wesselschmidt RL, Linette GP, Kanagawa O, Russel JH & Milbrandt J. Unimpaired thymic and peripheral T cell death in mice lacking the nuclear receptor NGFI-B (Nur77). *Science* 269, 532–535 (1995)
30. Patsalos A, Tzerpos P, Halasz L, Nagy G, Pap A, Giannakis N *et al.* The BACH1-HMOX1 regulatory axis is indispensable for proper macrophage subtype specification and skeletal muscle

regeneration. *J Immunol* 203, 1532–1547 (2019)

31. Sághy T, Köröskényi K, Hegedűs K, Antal M, Bankó, C, Bacsó Z *et al.* Loss of transglutaminase 2 sensitizes for diet-induced obesity-related inflammation and insulin resistance due to enhanced macrophage c-Src signaling. *Cell Death Dis* 10, 439 (2019)
32. Al-Zaeed N, Budai Z, Szondy Z & Sarang Z. TAM kinase signaling is indispensable for the proper skeletal muscle regeneration process. *Cell Death Dis* 12, 611 (2021)
33. Singlár Z, Ganbat N, Szentesi P, Osgonsandag N, Szabó L, Telek A *et al.* Genetic Manipulation of CB1 Cannabinoid Receptors Reveals a Role in Maintaining Proper Skeletal Muscle Morphology and Function in Mice. *Int J Mol Sci* 23, 15653 (2022)
34. Köröskényi K, Duró E, Pallai A, Sarang Z, Kloor D, Ucker DS *et al.* Involvement of adenosine A2A receptors in engulfment-dependent apoptotic cell suppression of inflammation. *J Immunol* 186, 7144–7155 (2011)
35. Lorenowicz MJ, Fernandez-Borja M & Hordijk PL. cAMP signaling in leukocyte transendothelial migration. *Arterioscler Thromb Vasc Biol* 27, 1014–1022 (2007)
36. Munoz-Canoves P, Scheele C, Pedersen BK & Serrano AL. Interleukin-6 myokine signaling in skeletal muscle: a double-edged sword? *FEBS J* 280, 4131–4148 (2013)
37. Tollefsen SE, Lajara R, McCusker RH, Clemmons DR & Rotwein P. Insulin-like growth factors (IGF) in muscle development: Expression of IGF-1 receptor, and an IGF binding protein during myoblast differentiation. *J Biol Chem* 23, 13810–13817 (1989)
38. Tontonoz P, Cortez-Toledo O, Wroblewski K, Hong C, Lim L, Carranza R *et al.* The orphan nuclear receptor Nur77 is a determinant of muscle size and muscle mass in mice. *Mol Cell Biol* 35, 1125–1138 (2015)
39. Kanzleiter T, Wilks D, Preston E, Ye J, Frankioudakis G & Cooney GJ. Regulation of the nuclear hormone receptor in muscle: Influence of exercise-activated pathways in vitro and obesity in vivo. *Biochim Biophys Acta* 1792, 777–782 (2009)
40. Maira M, Martens C, Batsché E, Gauthier Y & Drouin J. Dimer-specific potentiation of NGFI-B (Nur77) transcriptional activity by the protein kinase A pathway and AF-1-dependent coactivator recruitment. *Mol Cell Biol* 23, 763–776 (2003)
41. Yamaguchi H, Maruyama T, Urade Y & Nagata S. Immunosuppression via adenosine receptor activation by adenosine monophosphate released from apoptotic cells. *Elife* 3, e02172 (2014)
42. De Micheli AJ, Laurilliard EJ, Heinke CL, Ravichandran H, Fraczek P, Soueid-Baumgarten S *et al.* Single-cell analysis of the muscle stem cell hierarchy identifies heterotypic communication signals involved in skeletal muscle regeneration. *Cell Rep* 30, 3583–3595.e5 (2020)
43. Panicucci C, Raffaghello L, Bruzzone S, Baratto S, Principi E, Minetti C *et al.* eATP/P2X7R axis: An orchestrated pathway triggering inflammasome activation in muscle diseases. *Int J Mol Sci* 21, 5963 (2020)
44. Lynge J & Hellsten Y. Distribution of adenosine A1, A2A and A2B receptors in human skeletal muscle. *Acta Physiol Scand* 169, 283–290 (2000)

45. Lith SC, Gregoricchio S, van Tiel CM, van der Made I, Freire BM, Linder S, Jacobs S *et al.* Nuclear receptor Nur77 resolves the inflammatory response of macrophages primarily by regulating expression of AP-1 transcription factors and their target genes. *Nucleic Acid Res* 54, 808 (2026)
46. Suarez-Berumen K, Collins-Hooper H, Gromova A, Meech R, Sacco A, Dash PR *et al.* Pannexin 1 regulates skeletal muscle regeneration by promoting bleb-based myoblast migration and fusion through a novel lipid based signaling mechanism. *Front Cell Dev Biol* 9, 736813 (2021)
47. Sandona D, Gastaldello S, Martinello D & Betto R. Characterization of the ATP-hydrolysing activity of alpha-sarcoglycan. *Biochem J* 381, 105–112 (2004)
48. Christoffolete MA, Silva WJ, Ramos GV, Bento MR, Costa MO, Ribeiro MO *et al.* Muscle IGF-1-induced skeletal muscle hypertrophy evokes higher insulin sensitivity and carbohydrate use as preferential energy substrate. *Biomed Res Int* 2015, 282984 (2015)

Figures

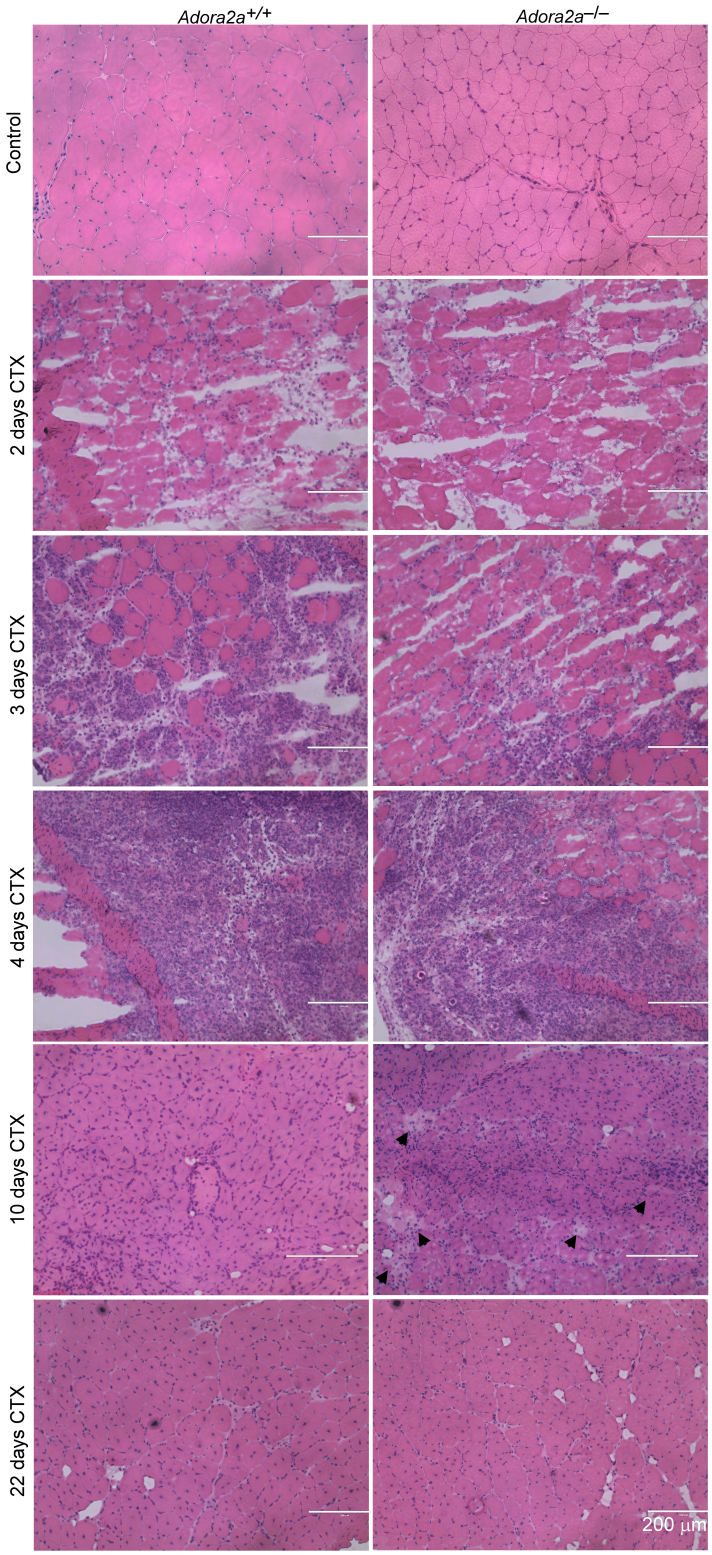


Figure 1

Time-dependent histological morphology of TA muscles following cardiotoxin-induced (CTX) injury in A2AR$^{+/+}$ and A2AR$^{-/-}$ mice. Muscle injury was induced by injecting 50 μl of 12 μM CTX into the TA muscles. Representative H&E-stained cross-sections of A2AR$^{+/+}$ and A2AR$^{-/-}$ TA muscles without treatment and at 2, 3, 4, 10, and 22 post-CTX–induced injury (n=4 in each group). Arrows indicate necrotic areas at day 10. Scale bars, 200 μm.

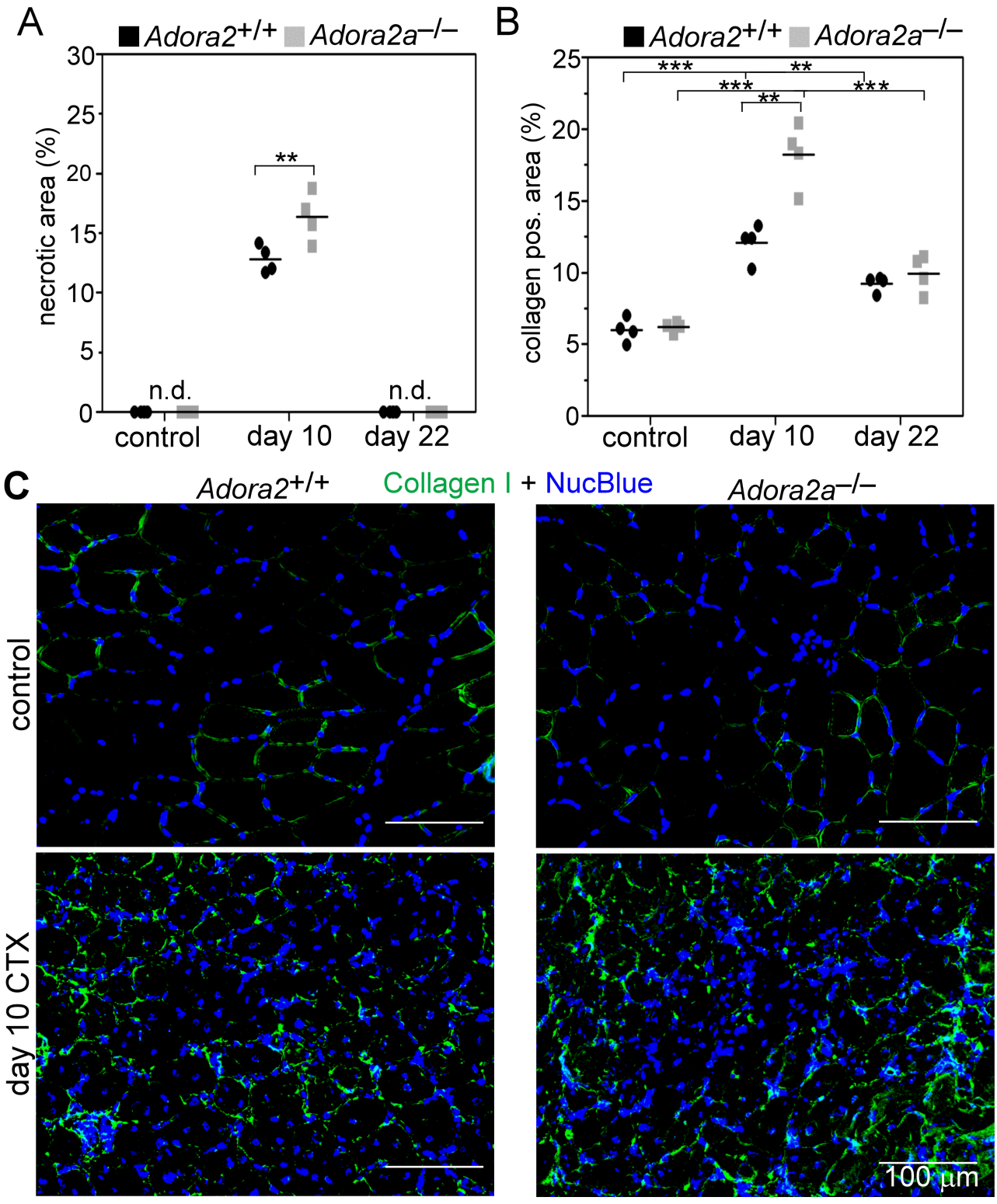


Figure 2

Delayed necrotic cell clearance and collagen deposition in TA muscles following CTX-induced injury in A2AR$^{-/-}$ mice. **A** Quantification of necrotic regions in the control and regenerating muscles of A2AR$^{+/+}$ and A2AR$^{-/-}$ mice at days 0, 10, and 22 post-CTX injury. **B** Quantification of collagen 1-positive regions in control and 10- and 22-day regenerating muscles of A2AR$^{+/+}$ and A2AR$^{-/-}$ mice. Data are expressed as mean and individual values, and statistical significance was determined by two-tailed Student's *t* test and

ANOVA. **$p < 0.01$, ***$p < 0.001$ n = 4. n.d., non-detected. **C** Representative immunofluorescence pictures of type 1 collagen (green) and NucBlue (blue) nuclear staining in control and 10-day regenerating TA muscles of $A2AR^{+/+}$ and $A2AR^{-/-}$ mice. Scale bars, 100 µm.

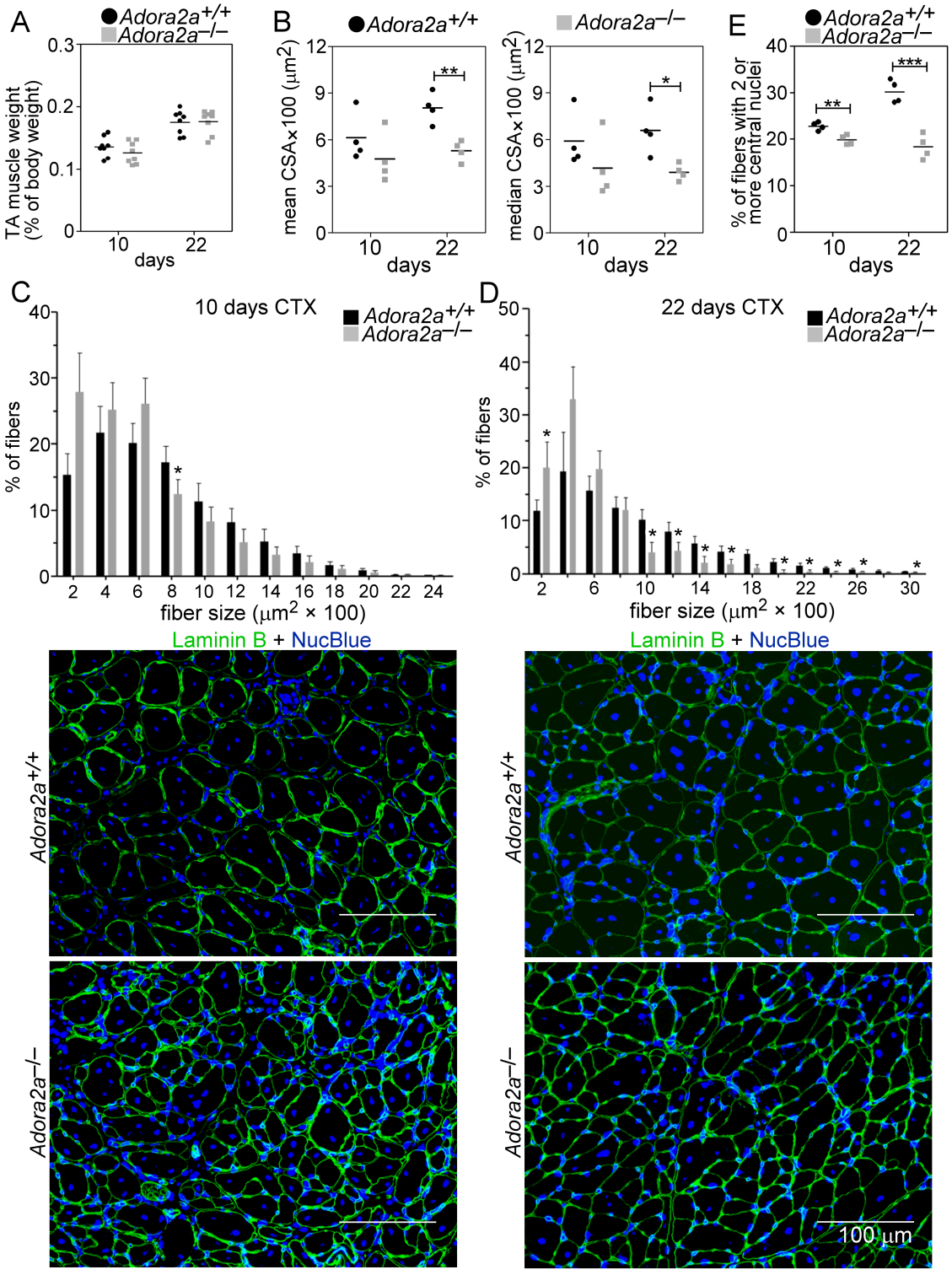


Figure 3

Impaired regeneration of TA muscle of A2AR$^{-/-}$ mice following CTX-induced injury. **A** Muscle/body weights, **B** mean and median myofiber cross-sectional areas (CSA), and **C, D** distribution of myofiber sizes in TA muscles of A2AR$^{+/+}$ and A2AR$^{-/-}$ mice at day 10 and 22 post-CTX–induced injury together with their representative immunofluorescence images of laminin (green) and NucBlue (blue) nuclear staining. Scale bars, 100 μm. 500 or more myofibers were analyzed in each sample using ImageJ software. Data are expressed as mean or median ± SD. **E** Percentage of newly formed myofibers containing two or more central nuclei in TA muscles of A2AR$^{+/+}$ and A2AR$^{-/-}$ mice at day 10 and 22 post-CTX–induced injury. Data are expressed as mean or median and individual values in panels A, B, and E (n = at least 4 samples), while as mean ± SD (n = 4) in panels C and D. Statistical significance was determined by two-tailed Student's *t*-test. *$p < 0.05$, **$p < 0.01$, ***$p < 0.001$.

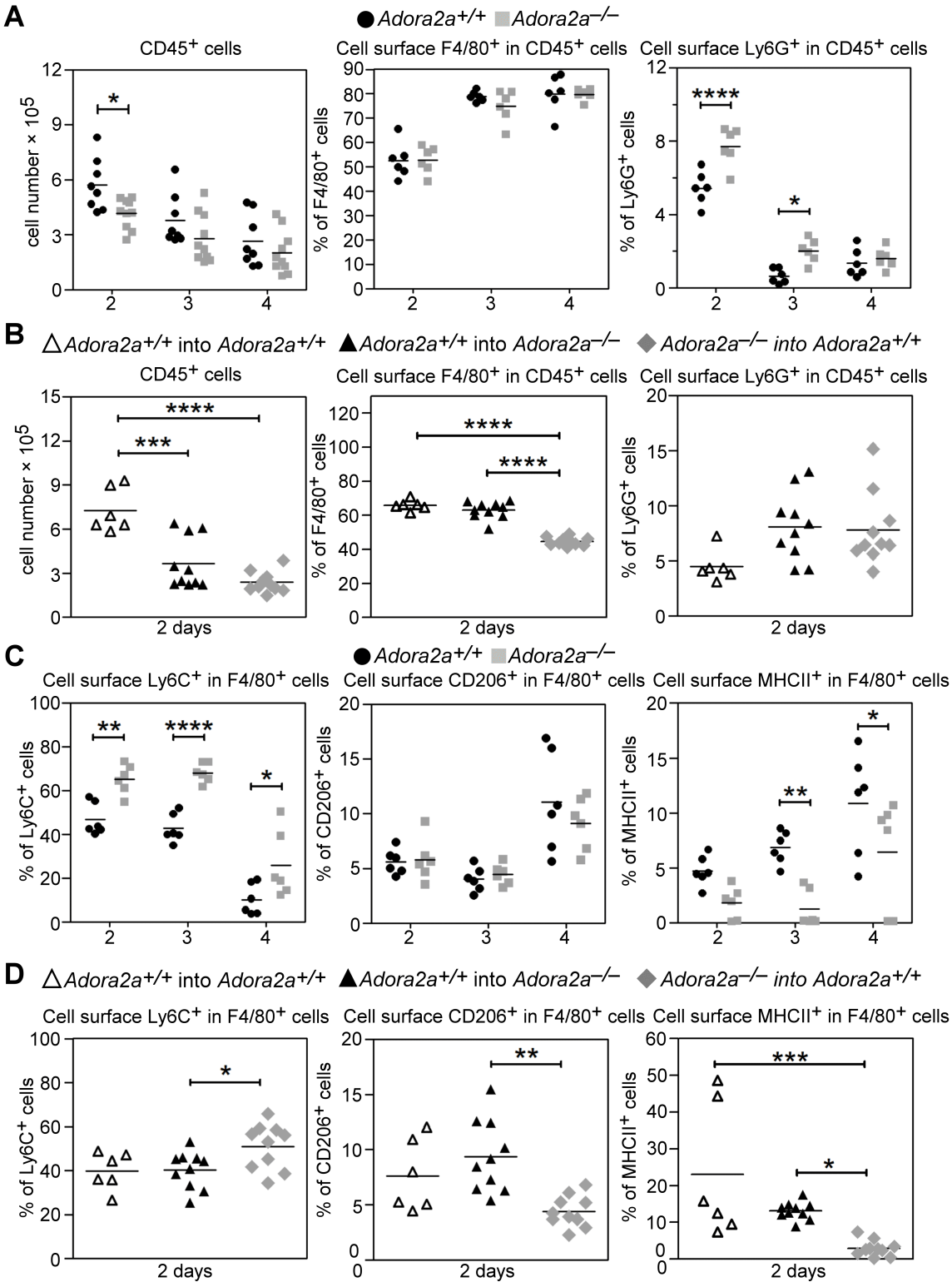


Figure 4

Decreased leukocyte transmigration and altered macrophage polarization in regenerating A2AR$^{-/-}$ TA muscles. **A** Alterations in the number of CD45^{+} leukocytes per injured muscle, percentage of anti-F4/80 antibody stained MΦs and that of Ly6G^{+} neutrophils within the CD45^{+} leukocyte population in A2AR$^{+/+}$ and A2AR$^{-/-}$ TA muscles during the first 4 days of regeneration following CTX-induced injury (n = at least

5 samples). **B** Alterations in the number of $CD45^+$ leukocytes per injured muscle, percentage of anti-F4/80 antibody-stained MΦs, and that of $Ly6G^+$ neutrophils within the $CD45^+$ leukocyte population in TA muscles following the indicated bone marrow transplantations at day 2 of regeneration following CTX-induced injury (n = at least 6 samples). **C** Alterations in the percentage of cell surface Ly6C, CD206, and $MHCII^{high}$ positive cells within the muscle-derived F4/80 positive macrophage population during the first 4 days of regeneration following CTX-induced injury (n = at least 5 samples). **D** Alterations in the percentage of cell surface Ly6C, CD206 and $MHCII^{high}$ positive cells within the muscle-derived F4/80 positive macrophage population following the indicated bone marrow transplantations at day 2 of regeneration following CTX-induced injury (n = at least 6 samples). Data are expressed as mean and individual values, and statistical significance was determined by two-tailed Student's *t*-test. **p* < 0.05, ***p* < 0.01, ****p* < 0.001, *****p* < 0.0001.

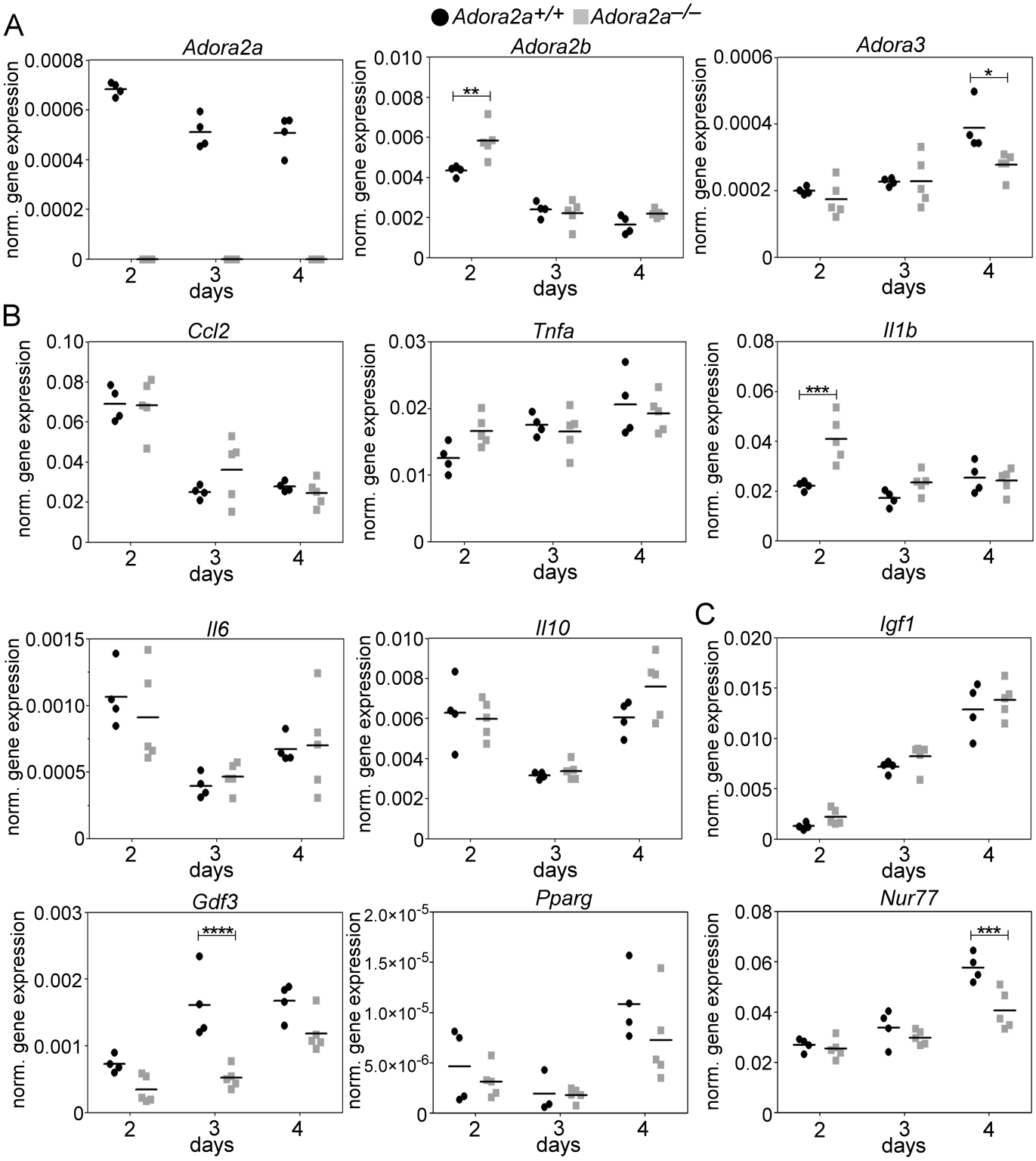


Figure 5

The loss of A2ARs results in altered expression of *Il1b* and *Gdf3* by muscle derived CD45^{+}cells. mRNA expressions **A** of various adenosine receptors **B** inflammatory markers and **C** growth and transcription factors in muscle-derived CD45^{+} cells isolated from A2AR$^{+/+}$ and A2AR$^{-/-}$ TA muscles at the indicated time points post-CTX injury detected by RT-qPCR (n = at least 4 samples). Data are expressed as mean

and individual values, and statistical significance was determined by two-tailed Student's *t*-test and ANOVA. *$p < 0.05$, **$p < 0.01$, ***$p < 0.001$, ****$p < 0.0001$.

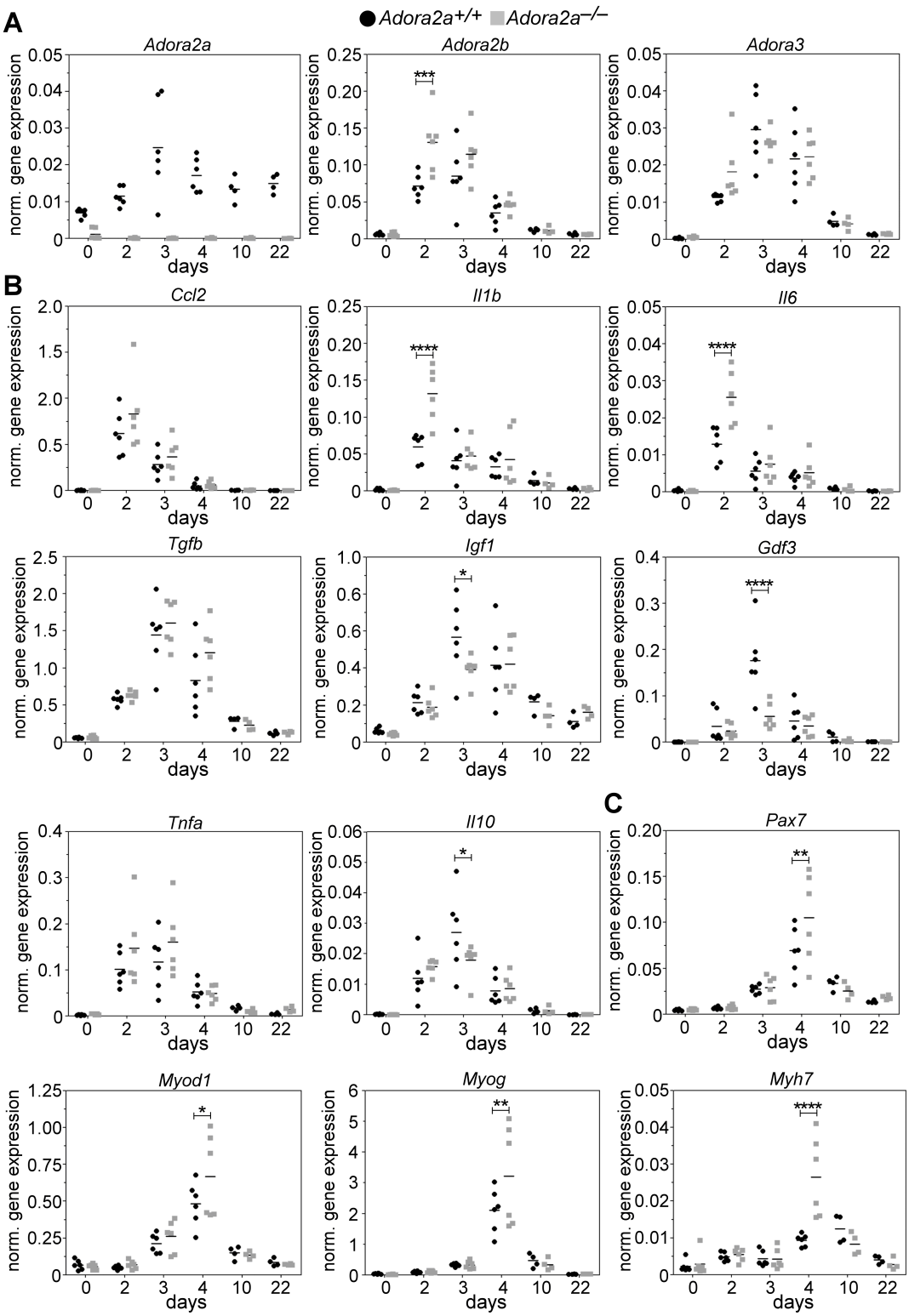


Figure 6

The loss of A2ARs results in enhanced expression of *Il1b* and *Il6*, decreased expression of *Igf1* and *Gdf3*, and increased number of proliferating SCs in TA muscles of A2AR$^{-/-}$ mice during regeneration. **A** mRNA

expressions of various adenosine receptors **B** various cytokines, and **C** SC proliferation- and differentiation-related genes in the TA muscles of $A2AR^{+/+}$ and $A2AR^{-/-}$ mice at the indicated time points post-CTX injury detected by RT-qPCR (n = 6). Data are expressed as mean and individual values, and statistical significance was determined by two-tailed Student's *t*-test. **p* < 0.05, ***p* < 0.01, ****p* < 0.001, *****p* < 0.0001.

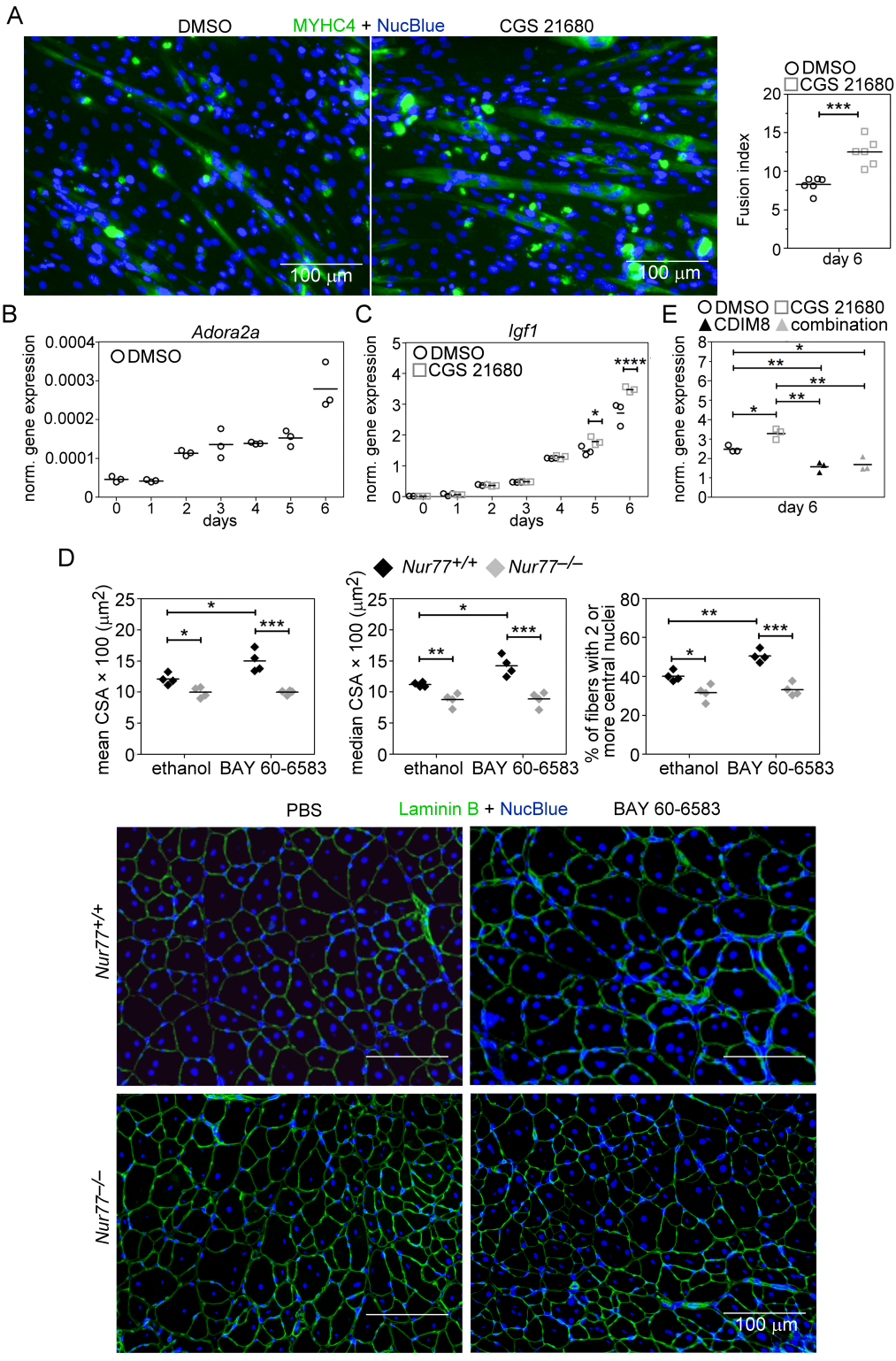


Figure 7

Stimulation of A2Rs enhances myoblast fusion both *in vitro* and *in vivo.* **A** Representative immunofluorescence images of myosin heavy chain 4 (MYH4) (green)- and NucBlue (blue)-stained C2C12 cells differentiated for 6 days in the presence and absence of 1 mM CGS21680, an A2AR agonist, and their fusion index. **B** Time-dependent mRNA expression of A2AR and **C** IGF-1 during the differentiation of the control and the CGS21680-treated C2C12 cells at the indicated time points post-CTX injury detected by RT-qPCR. **D** Fiber size and fusion index with the representative immunofluorescence pictures of laminin (green) and NucBlue (blue) stained TA muscles of *Nur77*$^{+/+}$ and *Nur77*$^{-/-}$ mice treated daily with BAY 60-6583 (2 mg/kg) or PBS during the first 6 days of regeneration detected at day 22 post-CTX injury. ImageJ software was used to examine 500 or more myofibers in each sample. Scale bars, 100 μm. **E** Alteration in *Igf1* expression of C2C12 cells treated for 6 days with CGS21680 in the presence and absence of C-DIM8 (5 mM), a Nur77 antagonist detected by RT-qPCR. Data are expressed as mean and individual values, and statistical significance was determined by two-tailed Student's *t* test. **p* < 0.05, ***p* < 0.01, ****p* < 0.001, *****p* < 0.0001 (n = at least 3 samples).

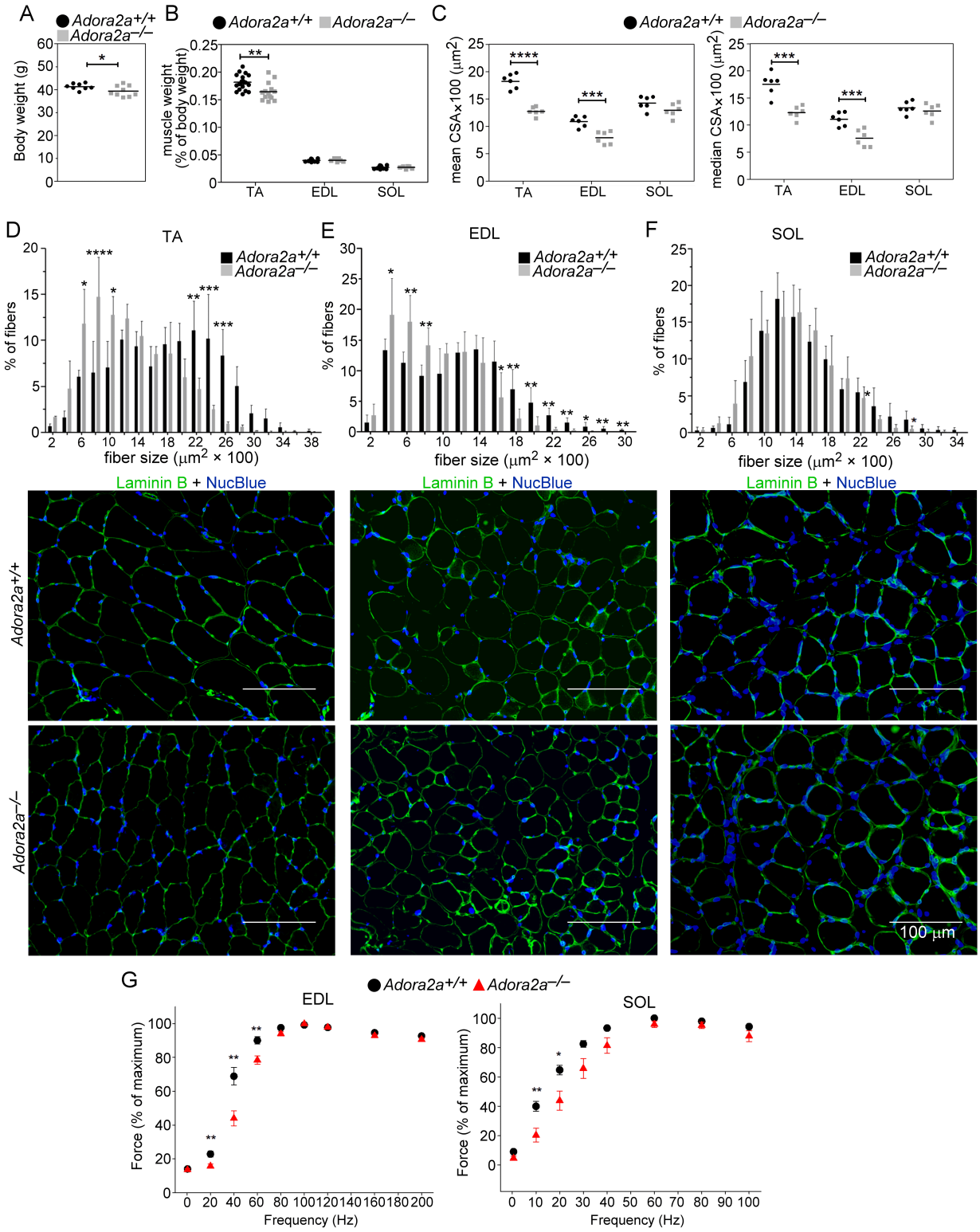


Figure 8

Loss of A2ARs alters the development of fast-twitch muscles. **A** Body weight and **B** muscle weight/body weight ratios in A2AR$^{+/+}$ and A2AR$^{-/-}$ mice. **C** Mean and median myofiber cross-sectional area (CSA) of the TA, EDL, and SOL muscles in A2AR$^{+/+}$ and A2AR$^{-/-}$ mice. Data are expressed as mean and individual values, and statistical significance was determined by two-tailed Student's *t*-test (n = at least 4 samples). Myofiber size repartition in **D** TA, **E** EDL, and **F** SOL muscles of A2AR$^{+/+}$ and A2AR$^{-/-}$ mice with their

representative immunofluorescence pictures of laminin (green) and NucBlue (blue) nuclear staining. ImageJ software was used to examine 500 or more myofibers in each sample. Scale bars, 100 µm. **G** Force-frequency relationship in EDL and in SOL muscles from $A2AR^{+/+}$ and $A2AR^{-/-}$ mice. Mean values ± SD are shown, and statistical significance was determined by two-tailed Student's *t*-test (n =at least 6 samples). *$p < 0.05$, **$p < 0.01$, ***$p < 0.001$, ****$p < 0.0001$.

Supplementary Files

This is a list of supplementary files associated with this preprint. Click to download.

- SupplementaryFigure1.tif
- SupplementaryFigure1legend.docx
- SupplementaryTable1.docx
- SupplementaryTable2.docx
- SupplementaryTable3.docx
- SupplementaryTable4.docx